Solar Phys (2019) 294:68
https://doi.org/10.1007/s11207-019-1453-3

Twin CME Launched by a Blowout Jet Originated from the Eruption of a Quiet-Sun Mini-filament

Ritika Solanki[1] · A.K. Srivastava[1] · Y.K. Rao[1] · B.N. Dwivedi[1]

Received: 24 December 2018 / Accepted: 9 May 2019 / Published online: 4 June 2019

Abstract We study a quiet-Sun blowout jet which was observed on 2014 May 16 by the instruments on board the *Solar Dynamics Observatory* (SDO). We find the twin CME as jet-like and bubble-like CMEs simultaneously as observed by LASCO C2 on board the *Solar and Heliospheric Observatory* (SoHO), and the *Solar Terrestrial Relation Observatory* (STEREO_A and STEREO_B/COR2). They are, respectively, associated with the eruption of the northern and southern sections of the filament. A circular filament is rooted at the internetwork region at the base of the blowout jet. The collective magnetic cancellation is observed by SDO/*Helioseismic and Magnetic Imager* (HMI) line-of-sight (LOS) magnetograms at the northern end of the filament, which makes this filament unstable and further makes it to erupt in two different stages. In the first stage, the northern section of the filament is ejected, and causes an evolution of the northern part of the blowout jet. This part of the blowout jet is further extended as a collimated plasma beam to form a jet-like CME. We also observe the plasma blobs at the northern edge of the blowout jet resulting from the Kelvin–Helmholtz instability in its twisted magneto-plasma spire. In the second stage, the southern section of the filament erupts in the form of a deformed/twisted magnetic flux rope which forms the southern part of the blowout jet. This eruption is most likely caused by the eruption of the northern section of the filament, which removes the confined magnetic field of the southern section of the filament. Alternative scenarios may be a magnetic implosion between these magnetic structures confined in a much larger magnetic domain. This eruption of the southern section of the filament further results in a bubble-like CME in the outer corona.

Keywords Sun: coronal blowout jet · Sun: coronal mass ejection (CME) · Sun: magnetic cancellation · Sun: Kelvin–Helmholtz instability · Sun: filament

Electronic supplementary material The online version of this article (https://doi.org/10.1007/s11207-019-1453-3) contains supplementary material, which is available to authorized users.

✉ R. Solanki
ritikas.rs.phy15@itbhu.ac.in

[1] Department of Physics, Indian Institute of Technology (BHU), Varanasi 221005, India

1. Introduction

Solar coronal jets are the magnetically-driven confined plasma eruptions which may be rooted in the lower solar atmosphere and further evolved in the solar corona. These dynamics occur in all solar environments such as the quiet Sun, an active region and coronal holes (*e.g.*, Shimojo *et al.*, 1996; Nisticò *et al.*, 2009; Panesar *et al.*, 2016; Raouafi *et al.*, 2016). Solar coronal jets can be divided in two classes based on the temperature range of the ejected plasma; we have: i) hot jets and ii) cool jets. In the hot jets, plasma is ejected into the solar corona along the open magnetic field lines as seen in UV, EUV, and X-ray wavelengths (*e.g.*, Shibata *et al.*, 1992, 2007; Shen *et al.*, 2012; Sterling *et al.*, 2015; Liu *et al.*, 2015; Shen *et al.*, 2017). The temperature range of the ejected plasma is $\approx 4 \times 10^6$ K for solar X-ray jets and $\approx 10^5$ K for EUV jets (*e.g.*, Shimojo *et al.*, 1996; Shimojo, Shibata, and Harvey, 1998). Jets observed in the Hα wavelength are termed cool jets, which are known as solar surges, having a typical temperature $\approx 10^4$ K (*e.g.*, Shibata *et al.*, 1982; Yokoyama and Shibata, 1995; Jiang *et al.*, 2007; Uddin *et al.*, 2012; Kayshap, Srivastava, and Murawski, 2013). However, cool coronal jets are also observed whose plasma is maintained at chromosphere, transition region (TR) temperatures (*e.g.*, Srivastava and Murawski, 2011; Kayshap *et al.*, 2013). Solar coronal jets have width ranges from 5×10^3 km to 1×10^5 km, height ranges from $\approx 10^4$ km to 4×10^5 km, and velocity ranges from 10 km s^{-1} to 1000 km s^{-1} (Shimojo *et al.*, 1996; Nisticò *et al.*, 2009). The widths of the jets can be determined by the length of the emerging bipoles as illustrated by Shen *et al.* (2011).

According to the magnetic topology of the coronal jets, they can be categorised in the following types: i) "Eiffel tower (ET) jets"; ii) "λ jets" (Nisticò *et al.*, 2009), *etc.* In ET jets, photospheric bipolar magnetic field reconnects with the ambient open unipolar magnetic field of opposite polarity at the top of a loop. In the λ-shaped jets, the bipolar magnetic field reconnects with opposite polarity open magnetic field at the footpoints. Solar jets are classified as anemone jets and two-sided loop jets based on their morphological structures and triggering mechanisms (*e.g.*, Shibata *et al.*, 1994; Yokoyama and Shibata, 1995; Tian *et al.*, 2017). There is another classification of solar coronal jets according to the standard model of the jet (Shibata *et al.*, 1992). The jets which follow the standard model of the jets are called standard jets, and the others which do not follow such characteristics are termed blowout jets. The concept of the blowout jets was first introduced by Moore *et al.* (2010) using Hinode/XRT observation of an X-ray jet. Blowout jets possess a broad spire and bright magnetic base arch, while standard jets have a narrow spire and dim magnetic base arch. In the blowout jet, the core field of the magnetic base arch carries the cool plasma ($\approx 10^4 - 10^5$ K) filaments. In the blowout jet, there is enough twist and shear in the base-arch field, so when the base-arch field and ambient field reconnect at the current sheet, this sheared and twisted arch field is also erupted. On the contrary, in the standard jet, the base arch is inactive and does not participate in the eruption (*e.g.*, Moore *et al.*, 2010, 2013; Sterling *et al.*, 2015). It should be noted that the blowout jet involves two reconnections, while the standard jet has only one reconnection. Sometimes, the eruption of the base-arch field takes the large form of the eruption and drags CMEs (Chen, 2011).

Hong *et al.* (2011) presented the observation of a blowout jet in a quiet Sun region where a mini-filament is ejected during an eruption and is associated with a mini-coronal mass ejection (CME). Shen *et al.* (2012) observed an quite region blowout jet which is associated with two CMEs as one is a bubble-like CME and another is a jet-like CME, where the bubble-like CME relates to the cool component of the jet and the jet-like CME relates to the hot component of the jet. Pucci *et al.* (2013) have done a comparative study of the blowout jet and standard jet and found that blowout jets have ten times higher magnetic energy as

compared to the standard jets. Adams *et al.* (2014) have analysed a blow-out jet event which originates from an on-disk coronal hole and shows different characteristics.

Miao *et al.* (2018) have analysed a coronal blowout jet eruption which is associated with an EUV wave at its leading top and complex CME structures (jet-like and bubble-like CMEs) where filament eruption is observed during the blowout jet. Shen *et al.* (2018c) have found a close relationship between the coronal jets and the EUV waves at different scales (spatial and temporal) in their observational event, where the EUV waves were propelled by the coronal jets. The observational results of Shen *et al.* (2018b) have shown the presence of EUV waves along with the coronal jets, where the EUV waves are generated by the lateral expansion of a loop system due to the coronal jet eruption. Shen *et al.* (2018a) have discussed the observations of arc-shaped EUV waves, a quasi-periodic fast propagating (QFP) wave, and a kink wave simultaneously with an active-region coronal jet eruption. Zhu *et al.* (2017) have observed an active-region blowout jet and investigated the 3D magnetic structure of the blowout jet and found that the kink instability is a possible triggering mechanism for this blowout jet. There are many research articles which deal with these interesting eruptive events and describe the different possible mechanisms of these eruptions (*e.g.*, Liu, 2008; Murawski, Srivastava, and Zaqarashvili, 2011; Chen *et al.*, 2015; Liu *et al.*, 2015; Alzate and Morgan, 2016). Wang *et al.* (1998) showed that EUV jets may be directly extended into the form of white-light jet-like CMEs. Coronal jets can cause multiple CMEs through interaction with remote structures (Jiang *et al.*, 2008) or through the self-evolution of coronal blowout jets (Shen *et al.*, 2012; Miao *et al.*, 2018). So far, studies on this issue are still very scarce.

In this paper, we have studied a blowout jet eruption observed on 2014 May, 16 which evolves due to the eruptions of the various segments of a quiescent filament. Here we observed the twin CME generation with this blowout jet. The jet-like CME is associated with the northern part of the blowout jet eruption and the bubble-like CME is driven from the eruption of the southern part of the blowout jet. Both parts of the blowout jet are associated with successive eruptions of the various segments of a filament. The K–H unstable blobs are also observed in the northern part of the blowout jet on its spire. The observational data and the analyses are described in Section 2. In Section 3, we illustrate the observational results and driving mechanisms of the observed blowout jet, and the kinematics of the twin CME. In Section 4, a discussion and conclusions are presented.

2. Analysis of Observational Data

2.1. Observations from *Solar Dynamics Observatory* (SDO)/*Atmospheric Imaging Assembly* (AIA)

We use high temporal and spatial *Solar Dynamics Observatory* (SDO; Pesnell, Thompson, and Chamberlin, 2012) data for the multi-wavelength study of the blowout jet. The *Atmospheric Imaging Assembly* (AIA; Lemen *et al.*, 2012) observes the full-disk Sun transition region and coronal emissions up to 0.5 $R_{\odot}$ above the solar limb. SDO/AIA provides full-disk images of the Sun in three UV wavelength bands (1600 Å, 1700 Å, 4500 Å) and in seven EUV wavelength bands (304 Å, 171 Å, 193 Å, 211 Å, 335 Å, 131 Å, 94 Å) covering the temperature range from 0.6 MK to 16 MK with 1.5″ spatial resolution, and 0.6″ pixel width. SDO/AIA captures full-disk images of the Sun with 12 s cadence in EUV filters and 24 s cadence in UV filters. We have taken the SDO/AIA data on 2014 May, 16 during the

time period of 03:30:00 UT – 05:10:00 UT for the selected region of 500″ to 900″ in the X-direction and −300″ to 0″ in the Y-direction. We have downloaded SDO/AIA data from the Joint Science Operation Center (JSOC).[1] Standard subroutines of SSWIDL (Freeland and Handy, 1998) are used for aligning and scaling AIA images as observed in different filters.

2.2. Observations from the *Solar Dynamics Observatory* (SDO)/*Helioseismic Magnetic Imager* (HMI)

We use *Helioseismic Magnetic Imager* (HMI; Scherrer *et al.*, 2012) data to examine the morphology and topology of the magnetic field at the footpoints of the observed blowout jet. SDO/HMI provides the full-disk line-of-sight (LOS) magnetic flux in the FeI 6173 Å spectral line. It has 45-second temporal resolution, 0.5″ pixel width and 1″ spatial resolution. We have analysed HMI magnetograms for the time period of 02:59:24 UT – 05:30:54 UT. The SDO/HMI data has been rotated and aligned with the SDO/AIA data by using the standard subroutines of SSWIDL.

2.3. Observations from the *Global Oscillation Network Group* (GONG)

We use GONG Hα (Harvey *et al.*, 2011) data to study the dynamics of the filament eruption. We have downloaded Hα data from GONG data archive.[2] This gives the full-disk Hα data with 1 minute cadence and 1″ spatial resolution in the 6563 Å wavelength.

2.4. Observations from the *Solar and Heliospheric Observatory* (SoHO)/*Large Angle and Spectrometric Coronagraph* (LASCO)

We use LASCO CME data obtained from the CME catalogue, which is available on the CDA website.[3] The *Large Angle and Spectrometric Coronagraph* (LASCO; Brueckner *et al.*, 1995) on board the *Solar and Heliospheric Observatory* (SoHO; Domingo, Fleck, and Poland, 1995) has identified coronal mass ejections (CMEs) in the images of the solar corona since 1996. LASCO has three telescopes named C1, C2, and C3. LASCO observes the white-light images of the solar corona from 1.1 $R_\odot$ to 30 $R_\odot$. The LASCO C2 coronagraph images the solar corona from 1.5 $R_\odot$ to 6 $R_\odot$, while the C3 coronagraph images the solar corona from 3.5 $R_\odot$ to 30 $R_\odot$. We use LASCO C2 and C3 data for a detailed scientific investigation of the twin CMEs as jet-like and bubble-like CME which are associated with the northern and southern part of the blowout jet.

2.5. Observations from the *Solar Terrestrial Relation Observatory* (STEREO)/*Sun Earth Connection Coronal and Heliospheric Investigation* (SECCHI)

We use data from the *Sun Earth Connection Coronal and Heliospheric Investigation* (SECCHI; Howard *et al.*, 2008) on board the STEREO-A and STEREO-B spacecraft to analyse the kinematics of the blowout jet, and the jet-like and bubble-like CMEs. We use the images from the *Extreme Ultraviolet Imager* (EUVI; Wuelser *et al.*, 2004) on SECCHI to determine the kinematics of the blowout jet, and the COR2 data of SECCHI for the kinematics

[1] See http://jsoc.stanford.edu to download SDO/AIA data.

[2] See https://gong.nso.edu/ to download GONG Hα data.

[3] See http://cdaw.gsfc.nasa.gov/CME_list to download LASCO data.

of the jet-like and bubble-like CMEs. The fields of view (FOV) of EUVI and COR2 are $1-1.7\ R_{\odot}$ and $2.5-15\ R_{\odot}$, respectively. We have downloaded the SECCHI data from the UKSSDC-STEREO archive.[4]

3. Observational Results

3.1. Source Location of the Blowout Jet Evolved due to the Quiet-Sun Filament Eruption

The blowout jet, which we have studied in the present paper was observed in the quiet-Sun region on 2014, May 16. This quiet-Sun region is near the western side of the NOAA active region AR12058 (S11W40), and lies in the fourth quadrant of the solar disk coordinates. The location of the blowout jet is $X_{\rm cen} = 660''$ and $Y_{\rm cen} = -150''$, and the initiation time is about 04:08:43 UT. This blowout jet is evolved due to the multiple stages of filament eruption which is rooted in the internetwork region of the quiet Sun. We will describe the physical picture of the unique plasma dynamics in the sub-sections below.

The multi-wavelength behaviour of the blowout jet is seen in the composite image of different SDO/AIA filters (*cf.* upper panel of Figure 1). We have plotted the composite image of the blowout jet and surrounding regions in AIA 1600 Å, AIA 304 Å and in the HMI line-of-sight (LOS) magnetogram at 04:11 UT. This image collectively shows the behaviour of the blowout jet simultaneously in the emissions from UV continuum to the transition region, and also the magnetic field polarities around its footpoint. The chosen field of view (FOV) for this composite image is $400'' \times 300''$ as $500''$ to $900''$ in the X-direction and $-300''$ to $0''$ in the Y-direction. In the composite image of the blowout jet, orange colour represents AIA 304 Å, green colour represents AIA 1600 Å, and blue colour represents HMI magnetogram.

The photospheric magnetic fields at the footpoint of the blowout jet and at its surroundings are shown in the HMI LOS (line-of-sight) magnetogram at 04:12:38 UT (*cf.* upper panel of Figure 2). The size of this magnetogram is $200'' \times 200''$ with the coordinates of $550''$ to $750''$ in X-direction and $-200''$ to $0''$ in the Y-direction. We see that there are various quiet-Sun magnetic networks in the neighbourhood of the blowout jet, and it originates with an internetwork quiet-Sun element where a circular filament is rooted (*cf.* bottom panels of Figure 3). The footpoint of the blowout jet is at the negative polarity (minority polarity) region in the vicinity of the positive polarity (majority polarity) region (*cf.* upper panel of Figure 2). For investigating the possible causes of the eruption of the filament and associated blowout jet and to understand the triggering mechanism for their eruptions, we examine the behaviour of the underlying magnetic field. In the initiation phase of the filament (*cf.* Figure 3), we have noticed the initial activity at the northern end of the filament which initiates the eruption of the filament. Therefore, we examine the time evolution of the magnetic flux around the northern end of the filament. The time variation of the negative magnetic flux and the positive magnetic flux at the northern end of the filament is shown in the bottom panel of Figure 2. The negative and positive magnetic fluxes are extracted from the box shown by the black solid line, which is overplotted on the HMI LOS (line-of-sight) magnetogram. The size of the box is $20'' \times 15''$ with the coordinates of $640''$ to $660''$ in the X-direction and $-135''$ to $-120''$ in the Y-direction. The magnetic field intensities are extracted for the observational period of 02:59:24 UT – 05:30:54 UT. The negative magnetic flux is of order

[4] See https://www.ukssdc.ac.uk/solar/stereo/data.html to download SECCHI data.

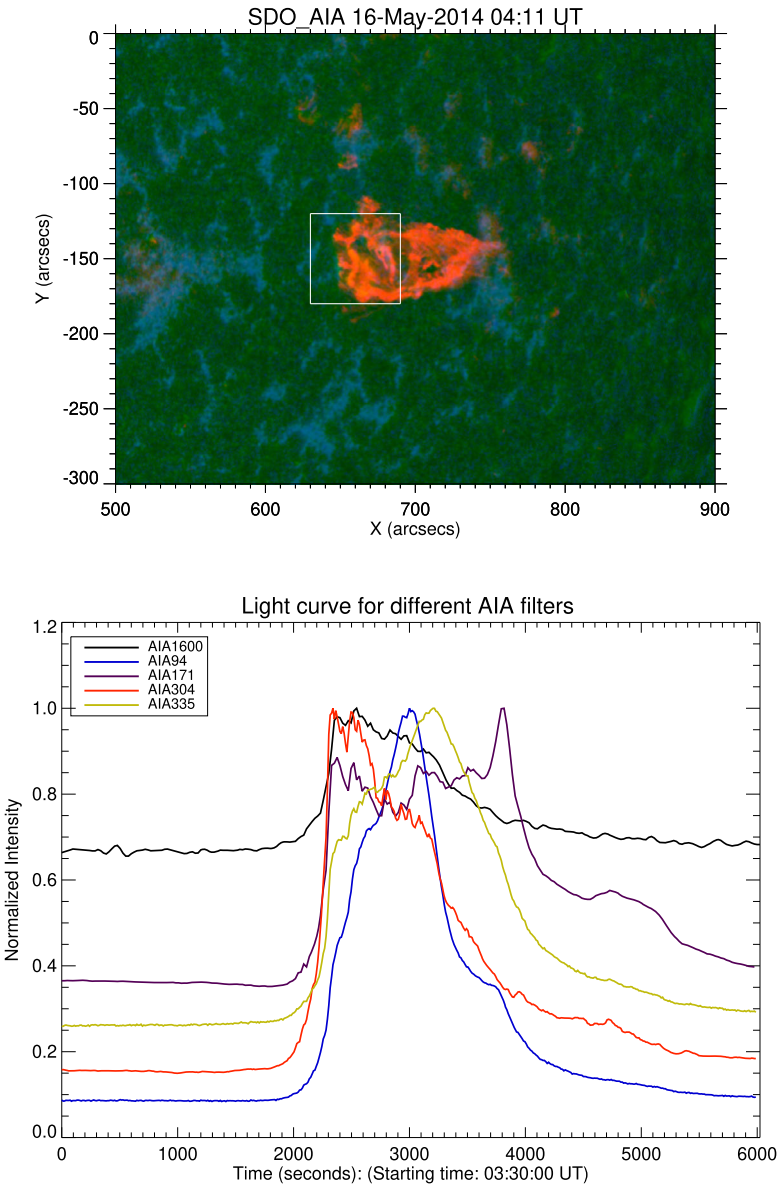

Figure 1 The *upper panel* shows the blowout jet eruption in the composite image of SDO/HMI, AIA 1600 Å, and AIA 304 Å at 04:11:00 UT. The *lower panel* shows the light curves obtained from different filters of SDO/AIA at the footpoint of the blowout jet.

10^{21} Mx while the positive magnetic flux is of order 10^{22} Mx. The blue dashed line overplotted on this figure indicates the starting time (03:59 UT) of the slow rising phase of the filament. We have noticed that the positive flux shows a declining trend while the negative flux shows an increasing trend. The changing behaviour of the negative and positive magnetic fluxes suggests that the negative flux is emerging and at the same time flux cancellation

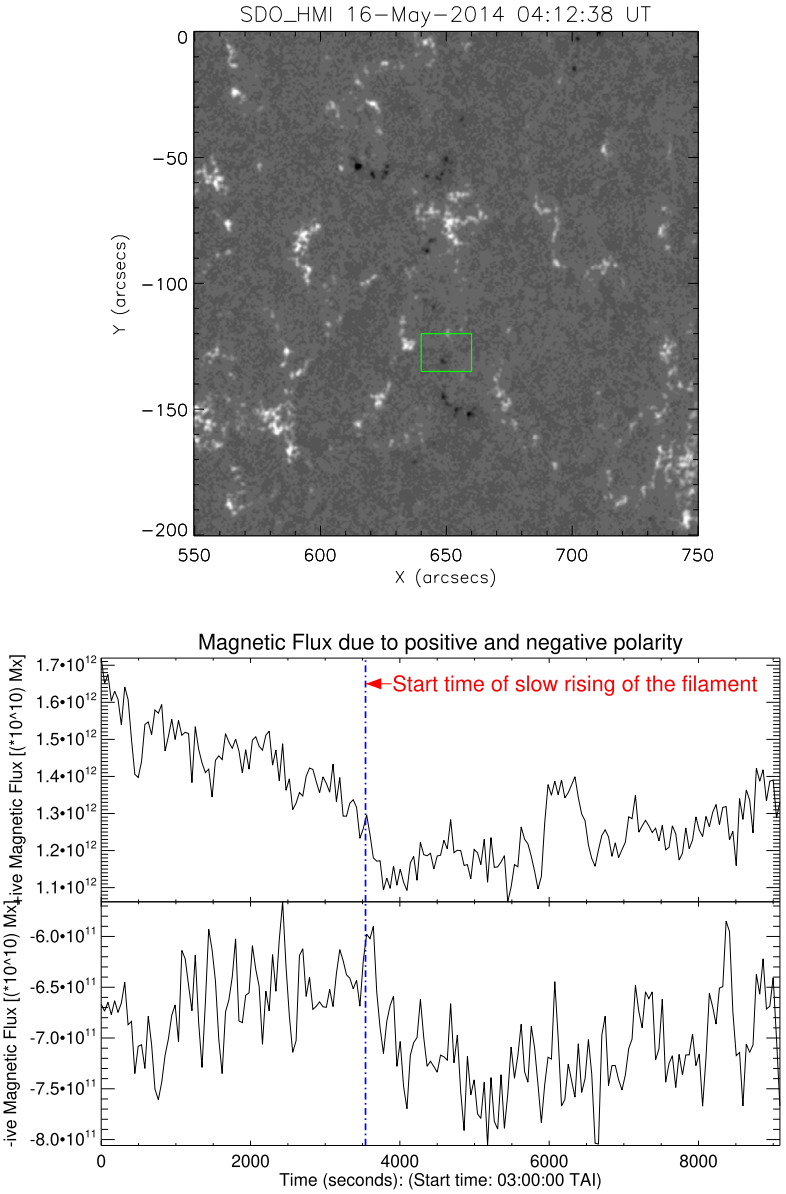

Figure 2 The *upper panel* shows a SDO/HMI line-of-sight (LOS) magnetogram at 04:12:38 UT. The *lower panel* shows the temporal evolution of positive and negative magnetic flux corresponding to the overplotted box on the HMI magnetogram of size $20'' \times 15''$ around the northern end of the filament.

between positive and negative flux takes place. This is a confirmation of the magnetic cancellation at the northern end of the filament, where filament eruption and activation of the northern part of the blowout jet are observed. Therefore, we can infer that the magnetic flux cancellation at the northern end of the filament makes it eruptive in multiple parts, which further evolve during the blowout jet eruption.

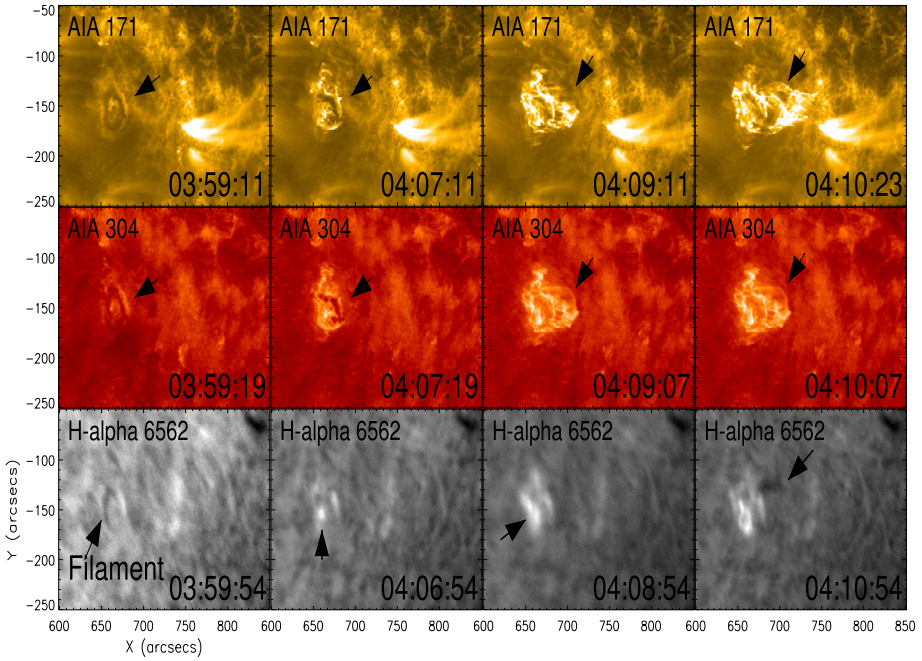

Figure 3 The complete picture of the initiation of the initial phase of the blowout jet due to the activation of circular filament. The northern section of the filament starts to eject at 04:10:54 UT in Hα and evolves the eruption of the blowout jet (*cf.* Movie 1; *top-most row*).

3.2. Time–intensity Profile at the Base of the Blowout Jet in Different SDO/AIA Filters

The lightcurve is plotted in different SDO/AIA filters for analysing the behaviour of the EUV brightening which is observed at the base of the blowout jet (*cf.* bottom panel of Figure 1). The intensity is extracted in different SDO/AIA filters from the box with the white solid line which is overplotted on the composite image of SDO/AIA filters over the observational period of 1 hour 40 minutes from 03:30:00 UT to 05:10:00 UT. The white-line box size is $60'' \times 60''$ and has the coordinates $630''$ to $690''$ in the X-direction and $-180''$ to $-120''$ in the Y-direction. The light curve is plotted in the AIA 1600 Å line (shown by black colour), and AIA 304 Å (shown by red colour), AIA 171 Å (blue colour), AIA 335 Å (yellow colour), AIA 94 Å (violet colour) between the normalised intensity (maximum intensity/mean intensity) and the observational period of the evolution of the blowout jet. The light curves in the different SDO/AIA filters show different behaviours *i.e.*, there is no identical intensity peak for all filters. The intensity has its peak value in AIA 1600 Å, and AIA 304 Å earlier in comparison to other filters. For these two filters the intensity peaks show nearly the same behaviour as the first peak observed at about 04:08:18 UT and the second peak is observed at about 04:11:36 UT. This demonstrates that cool plasma is firstly evolved during the formation of the blowout jet's spire. This is an opposite scenario to typical coronal jets where the hot plasma evolves first and the cool plasma thereafter (*e.g.*, Jiang *et al.*, 2007; Nishizuka *et al.*, 2008; Solanki, Srivastava, and Dwivedi, 2018). The current observations reveal that some distinct mechanism is at work in the formation of this quiet-Sun blowout jet other than the typical magnetic reconnection in the corona. The most likely scenario is based

on collective small-scale flux emergences and subsequent cancellation in the neighbourhood of the boundary of the magnetic network (*cf.* Figure 2). This launches the bulk plasma flows into the pre-existing blowout jet spire's magnetic field in the upward direction. The cool plasma has the temperature range $\approx 10^4 - 10^5$ K. After these two filters the intensity attains its peak value in AIA 94 Å and in AIA 335 Å at about 04:20:00 UT and 04:23:18 UT, respectively. AIA 171 Å shows a slightly different kind of behaviour in the intensity plot as there are many peaks in the light curve of AIA 171 Å, first two small peaks which match well with AIA 1600 Å and AIA 304 Å at 04:08:18 UT and at 04:11:36 UT with lower intensity. The intensity attains its peak value at about 04:33:18 UT in AIA 171 Å. In the light curve, a shift is observed in the intensity peaks of different SDO/AIA filters, which emphasises the time-lagging behaviour of the evolution of multi-temperature plasma throughout the entire period of the evolution of the blowout jet at different time epochs. This time-lagging behaviour indicates the presence of flare evolution at the base of blowout jet. A weak flare is observed at about 04:08 UT near the northern side of the blowout jet and the filament, which accelerates the plasma in the eruption. We relate this weak flare with the network flare (Krucker *et al.*, 1997; Krucker and Benz, 2000).

3.3. Evolution of the Blowout Jet due to the Eruption of Segments of a Filament as Seen in Different SDO/AIA Filters and GONG Hα

The initiation phase of the blowout jet in different SDO/AIA filters as seen in AIA 304 Å, AIA 171 Å and in GONG Hα 6563 Å indicates the presence of cool plasma and the filament at the base of the blowout jet (*cf.* bottom panels of Figure 3). This filament is embedded in the internetwork region, which can be seen in the first image of the bottom panel in Hα at 04:03:54 UT. In the GONG Hα observations this filament is a circular shaped structure. Firstly a slow rise is observed in the filament. The cool plasma and unstable filament move up and the jet bright points are created at the filament root at 04:08:54 UT, which is a network flare (see Figure 3). The filament erupts at about 04:10:54 UT. In the initiation phase, filament shows slow rise, ejection and evolution of the blowout jet. The evolution of the blowout jet can be seen in animation Movie 1.

The filament is ejected in two stages as the circular-shaped structure of the filament divides into two parts. In the first stage, the eruption of northern part of the filament (first part) takes place and drives the blowout jet (*cf.* Figure 4). The hot plasma escapes and moves linearly along the open magnetic field lines and form a broad and complex jet-like spire (*cf.* the northern part of the eruptions in Figure 4). In the blowout jet, the eruption of the northern side of the blowout jet is most activated in its primary phase, and significant plasma dynamics is seen along it (*cf.* Figure 4). The formation of plasma blobs is clearly evident in this part, which we will describe in Section 3.4.

3.4. Formation of Plasma Blobs in the Northern Spire of the Blowout Jet

We have found plasma blobs at the edge of the northern spire of the blowout jet. The formation and evolution of these plasma blobs can be seen in the time-sequence images of AIA 304 Å in Figures 5 and 6. The selected FOV for these images is $80'' \times 50''$ from $670''$ to $750''$ in the X-direction and from $-150''$ to $-100''$ in the Y-direction in Figure 5. These plasma blobs are identified as B1, B2, B3, B4 in the middle panel of Figure 5. The total time-durations of these plasma blobs are about 3 min 48 sec. The northern side of the blowout jet where these plasma blobs are formed is highlighted with the blue-lined box in Figure 6.

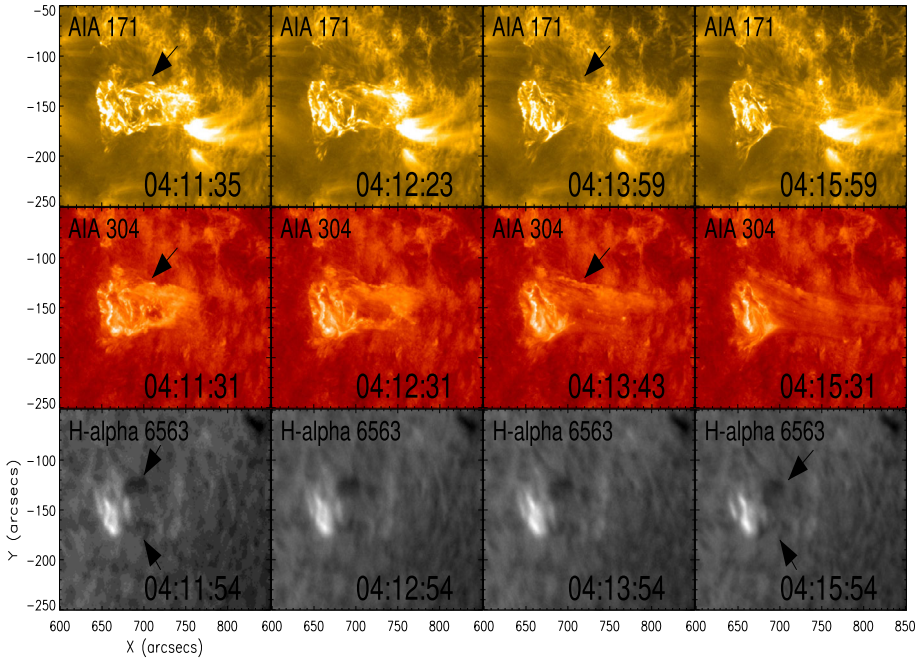

Figure 4 Evolution of northern part of the blowout jet in the time-sequence images of AIA 304 Å, AIA171 Å, and Hα. The hot plasma escapes and forms a broad, complex, northern spire of blowout jet which shows linear motion, and exhibits the formation of plasma blobs (*cf.* Movie 1; middle row).

The bottom panel of Figure 6 shows a zoomed-in picture of the plasma blobs. The formation of the plasma blobs results from the Kelvin–Helmholtz (K–H) instability. These hot and high-density plasma blobs are moving along the northern spire of the blowout jet. The K–H instability arises due to the shear flows between the high speed blowout jet and the steadily moving local plasma and result in the formation of magnetic islands. These islands take the form of plasma blobs at the time of the evolution.

We have analysed the velocity field at the northern side of the blowout jet using Fourier local correlation tracking (FLCT; Fisher and Welsch, 2008) method (*cf.* right panel of Figure 7). The velocity field is analysed at the northern side of the blowout jet corresponding to the box which is overplotted on the AIA 1600 Å image having the coordinates of 500″ to 900″ in the X-direction and −300″ to 0″ in the Y-direction (*cf.* left panel of Figure 7). We have selected two HMI LOS magnetograms, at 03:37:36 UT and at 04:14:08 UT (at the timing of the onset of the blowout jet) to estimate the flow-field velocity field. In the right panel of Figure 7, we see the base image of the HMI magnetogram at 03:37:36 UT and the velocity field is shown by orange arrows overplotted on the base image taken from the HMI magnetogram at 04:14:08 UT.

It is clearly evident that the clockwise plasma flow is centred at that particular quiet-Sun region where the blowout jet originates. The right panel of Figure 7 shows the partial field of view at the footpoint of the northern side of the blowout jet ($X = 640'' - 710''$, $Y = -125'' - -100''$). The yellow contour which is overlaid on the HMI magnetogram shows the AIA 304 Å intensity. It is clear that the clockwise shearing-flow field is acting at the footpoint of the northern side of the blowout jet, which further launches the right-handed twist in the entire overlying plasma column/spire associated with the blowout jet. When this clockwise shear-

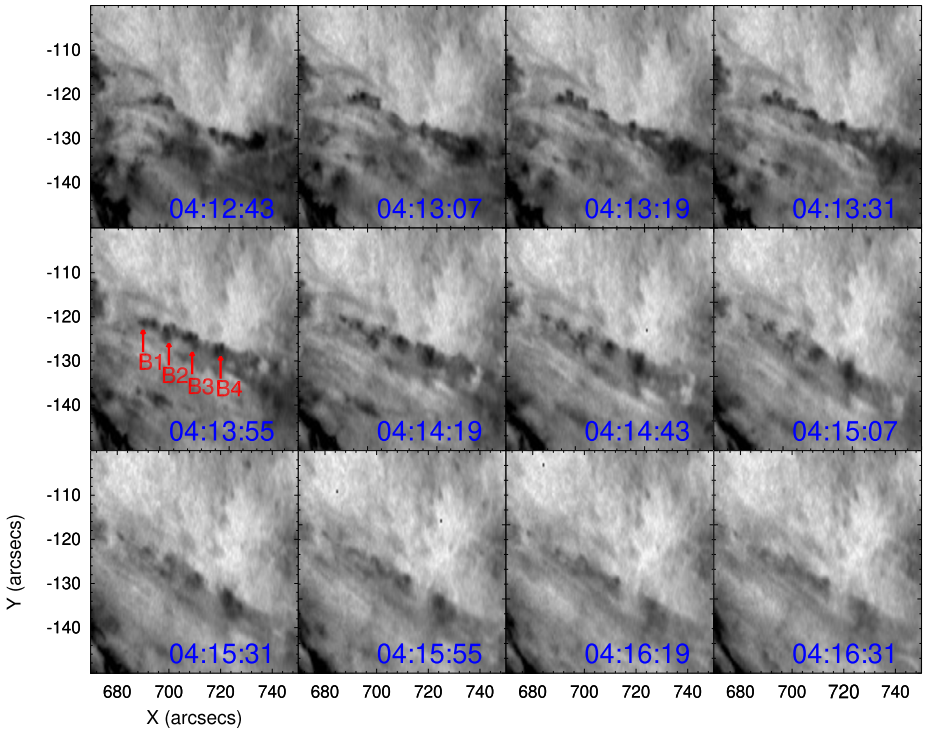

Figure 5 The plasma blob formation at the northern side of the blowout jet is shown in the time-sequence images of SDO/AIA 304Å.

ing flow field moves further and interacts with the local stationary plasma field, it causes the K–H instability which results in the formation of four plasma blobs (B1, B2, B3, B4). The plasma blobs are less visible in the AIA 304 Å channel due to the smaller spatial and time resolutions data. The northern spire of the jet also exhibits untwisting/rotational motion. The jet's spire shows the estimated twist is about 1 – 1.5 turns (or $2\pi - 3\pi$). Our twist value is in good agreement with the results of Pariat, Antiochos, and DeVore (2009), who show that, for the driving of a solar coronal jet the threshold value of the twist is 1.4 turns (2.8π). Our finding of the K–H unstable plasma blobs in the rotating/untwisting spire of the blowout jet supports the numerical results of Ni *et al.* (2017), Zhelyazkov *et al.* (2018) and Zhelyazkov and Chandra (2018). This K–H unstable northern plasma spire further moves into a higher coronal region and drives a jet-like CME, which we will discuss in Section 3.7.

3.5. Kinematics of the Northern Part of the Blowout Jet

We have conducted a height–time analysis of the northern part of the blowout jet. To calculate the height of the blowout jet, we have used the tie-pointing method of Inhester (2006). In this method the triangulation technique between the different view points of STEREO_A and SDO/AIA is used. In this triangulation technique, scc_measure.pro is used which is available in the solarsoft library for estimation of the real height of the blowout jet. We have calculated the height of the blowout jet by tracking the tip of the blowout jet in two different view points of STEREO_A and SDO/AIA (*cf.* the upper panel of Figure 8). In the bottom

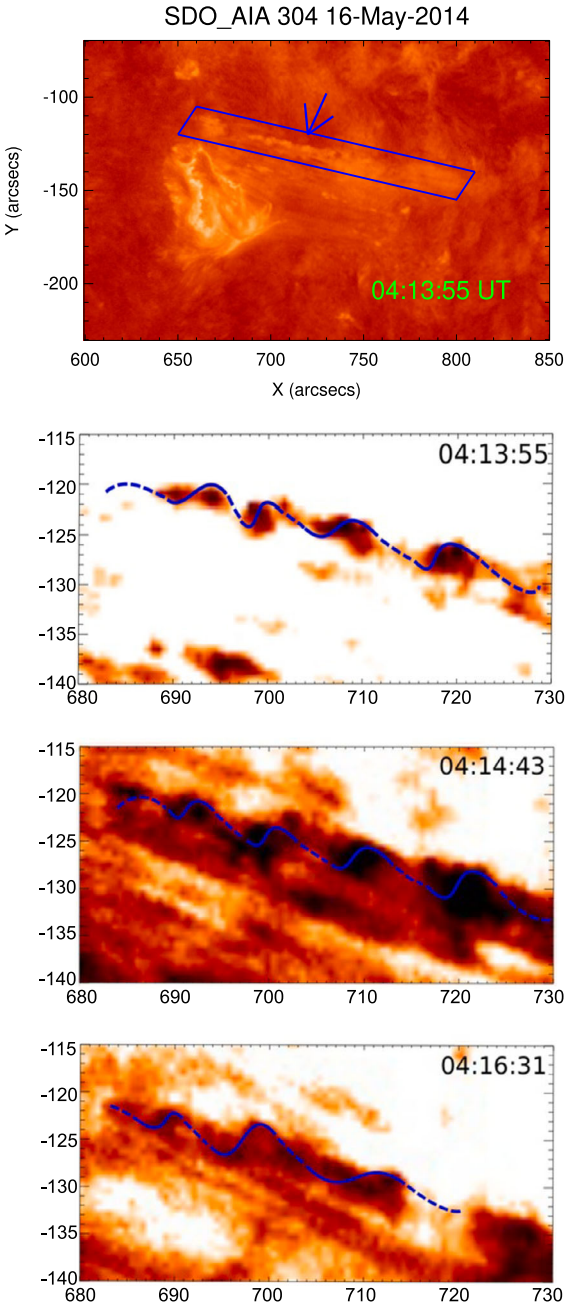

Figure 6 In the *upper panel* the *blue-line box* highlights the northern side of the blowout jet, where formation of plasma blobs takes place. In the *bottom panel* images of SDO/AIA 304 Å show the evolution of plasma blobs as well as launch of the magnetic twists at different epochs.

panel of Figure 8, the height of the jet has been tracked using its tip starting at 04:06:09 UT, when the jet is clearly visible in both instruments (SDO/AIA 304 Å and STEREO_A EUVI 304 Å), while the initiation of jet takes place at 03:59 UT. We have calculated the height (in $R_{\odot}$) of the blowout jet at ten different times (in UT): 04:06:19, 04:10:31, 04:14:07, 04:15:31, 04:16:19, 04:16:31, 04:20:31, 04:25:31, 04:26:15, and 04:30:30. With this height–time ar-

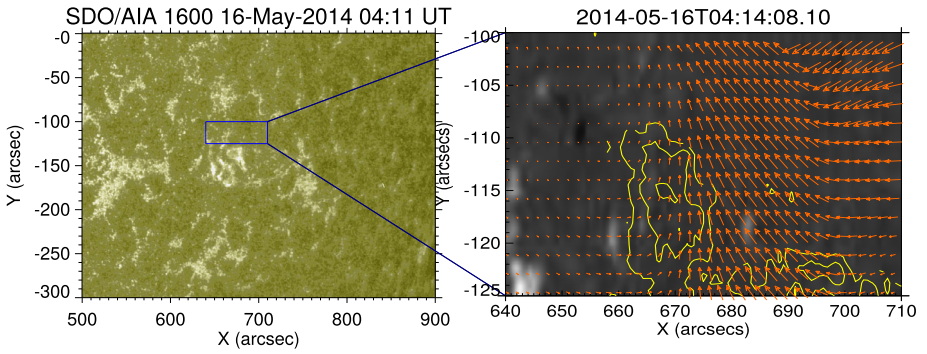

Figure 7 The *left panel* shows the AIA 1600 Å image at 04:11 UT, a *blue solid line box* is overplotted on it which indicates the northern side of the blowout jet. The *right panel* shows the velocity field at the northern side of the blowout jet, where clockwise plasma shearing motion is evident.

ray, we have calculated the velocity of the blowout jet, which is ≈ 325 km s^{-1} (*cf.* bottom panel of Figure 8). The calculated acceleration for this blowout jet is ≈ -0.30 km s^{-2} which is estimated by the second order fitting in the height–time plot of the blowout jet.

3.6. Eruption of the Southern Part of the Filament and Associated Blowout Jet

After the activation and eruption of the northern section of the filament and associated segment of the blowout jet, the southern section of the filament also erupts in the form of a twisted/deformed flux rope (*cf.* Hα, AIA 304 Å images in bottom and middle panel of Figure 9 which shows the second stage of the eruption, *cf.* AIA 171Å images of Figure 9). The eruption of the southern part of the filament can be seen in the animation Movie 1. This deformed/twisted magnetic flux rope moves further and releases its helicity and forms a rotating plasma spire at the southern part of the blowout jet. The eruption of the northern section of the filament destabilises and removes the local magnetic field configurations and induces the eruption of the southern section of the filament. Alternatively we may adopt the magnetic implosion physical mechanism for the initiation of the eruption of the southern section of the filament. It may occur between neighbouring magnetic structures confined by a large magnetic structure (Hudson, 2000; Liu, Wang, and Alexander, 2009; Shen, Liu, and Su, 2012). At the magnetic implosion site, the eruption takes place when the upward magnetic pressure decreases resulting in contraction of the overlying field and free magnetic energy release.

3.7. Jet-like and Bubble-like Twin CME

In this analysed event, we have found the generation of a twin CME associated with the blowout jet eruption. The northern part of the filament erupts first and causes the evolution of the coronal blowout jet, which may also be subject to the K–H instability. Thereafter, the southern part of the filament also erupts in the form of a magnetic flux rope, and forms the full blowout jet eruption.

The northern and southern segments of the filament may be confined by the same magnetic field system. Magnetic flux cancellation occurred at the northern end of the filament which makes this filament unstable and leads it to erupt in different stages. In a first stage the northern segment of the filament ejects and initiates the eruption of the northern part of

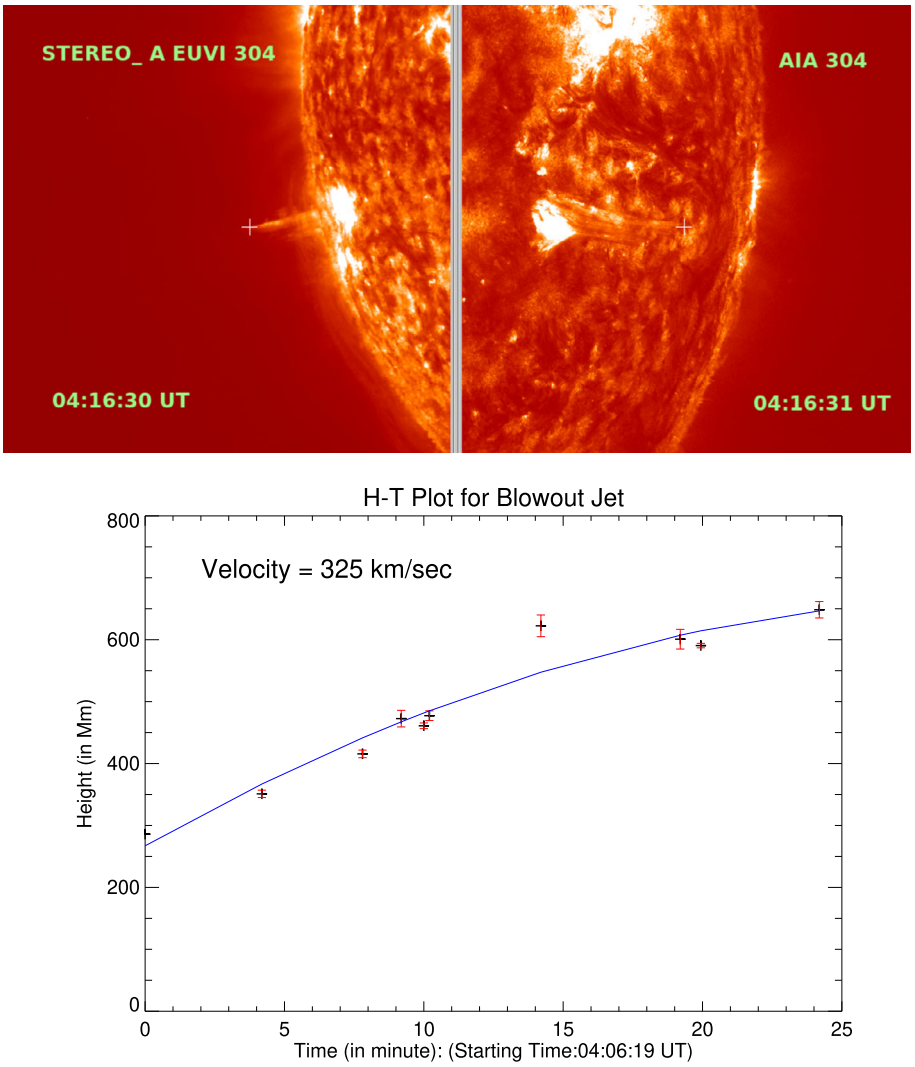

Figure 8 In the *upper panel* the tip of the blowout jet is tracked simultaneously in STEREO_A EUVI 304 Å and AIA 304 Å by using the triangulation technique. The *bottom panel* shows the height–time plot for the blowout jet.

the blowout jet. The northern part of the blowout jet further drags the first CME which is a jet-like CME. This jet-like CME is the extension of the collimated plasma beam which is generated by the external magnetic reconnection (Shen *et al.*, 2012).

The eruption of the northern section of the filament removes the confined magnetic field of the southern section of the filament and induces the eruption of the southern section of the filament. Alternatively we may adopt the magnetic implosion mechanism for the eruption of the southern section of the filament. The eruption of the southern section of the filament forms the full blowout jet eruption and causes the second CME which is a bubble-like CME.

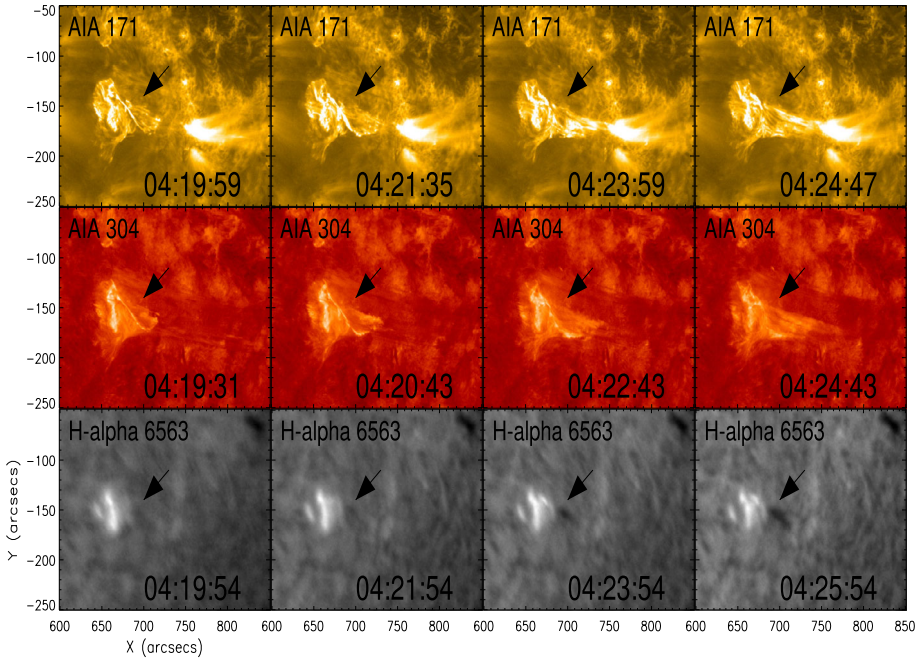

Figure 9 In the second stage, the eruption of southern section of the filament occurred in the form of twisted/deformed magnetic flux rope. This enables the formation of a rotating plasma spire of the southern segment of this blowout jet (*cf.* Movie 1; *bottom row*).

The line-of-sight (LOS) evolution of these twin CMEs are shown in running difference images of the SoHO/LASCO C2 coronagraph (*cf.* Figure 10). The dynamics of these two CMEs can be seen in the animation Movie 2. We have used the multi-scale Gaussian normalisation method of Morgan and Druckmüller (2014) in making these running difference images. We have marked the jet-like CME and the bubble-like CME in Figure 10 for the image of 05:12:05 UT. The bubble-like CME has the typical three-part structure of a bright core which consists of cool plasma material of the filament, a dark cavity and the bright front of the CME. The bright core is at the northern side of the dark cavity. Generally the bright core resides at the centre of the dark cavity and the CME. The first appearance of the CME in the LASCO C2's FOV is observed at about 04:38:53 UT. The spatial and the temporal relationship between the twin CME and the northern as well as the southern part of the jet eruption relates to the eruptions of the northern and southern sections of the filament which determine the jet-like and the bubble-like CME.

3.8. Kinematics of the Jet-like and Bubble-like CME

We have performed the height–time analysis for the study of the kinematics of the jet-like and bubble-like CMEs. We have applied the same method for height–time measurements of these twin CMEs. We have measured the projected height for these CMEs with respect to the centre of the solar disk by using the tie-pointing method of the Inhester (2006). We have tracked the tip of the CMEs in STEREO_A COR2 and STEREO_B COR2 simultaneously with the help of the triangulation technique. The separation angle between STEREO_A and STEREO_B on 2014 May 16 at 04:00 UT is about 36°. Since the longitude angle is high in

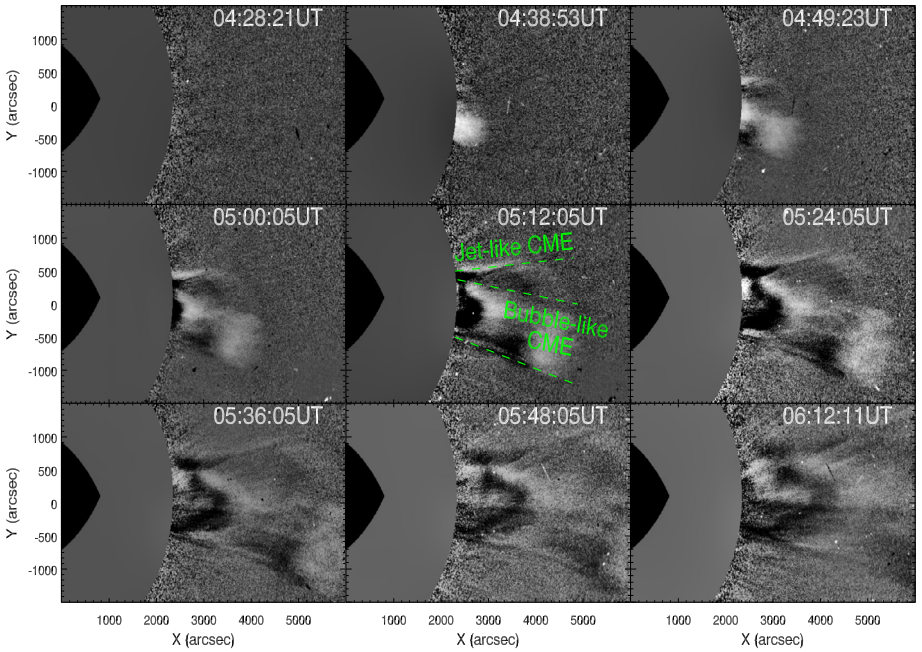

Figure 10 Twin CME evolution at different times as observed in SoHO/LASCO C2 coronagraph (*cf.* Movie 2). The northern part of the blowout jet drags the jet-like CME and the eruption of the southern section of the filament causes the bubble-like CME.

these measurements, we have estimated the projected height of the twin CME. In the case of a jet-like CME, we have estimated the projected height at five different times as 05:09:15 UT, 05:24 UT, 05:39 UT, 05:54 UT and 06:09:15 UT. At each time we have tracked the tip of the CME (measurement of projected height) at ten times to estimate the underlying uncertainty in the measurements. With these data sets of projected height and time we have plotted the height–time plot for a jet-like CME (*cf.* Figure 11). The calculated velocity for a jet-like CME is about 619 km s^{-1}. We have performed second order fitting on the height–time plot to calculate the acceleration of the CME and get the acceleration value 0.35 km s^{-2} for the jet-like CME.

In the case of a bubble-like CME we have estimated the projected height at 04:54 UT, 05:09:15 UT, 05:24 UT, 05:39 UT, 05:54 UT, 06:09:15 UT, 06:24 UT, and 07:09:15 UT. With the projected height and time data sets we have plotted the height–time plot for a bubble-like CME and calculated the velocity of the bubble-like CME (*cf.* Figure 12). The calculated velocity is about 620 km s^{-1}. The calculated acceleration is about -0.031 km s^{-2}. We have performed the second order fitting on the height–time plot of a bubble-like CME to get the value of this negative acceleration.

4. Discussion and Conclusions

There are many observational results which deal with the blowout jet eruption from the active region of the Sun and their different characteristics and triggering mechanisms. Li *et al.* (2015) observed an active-region blowout jet which is associated with a CME and a

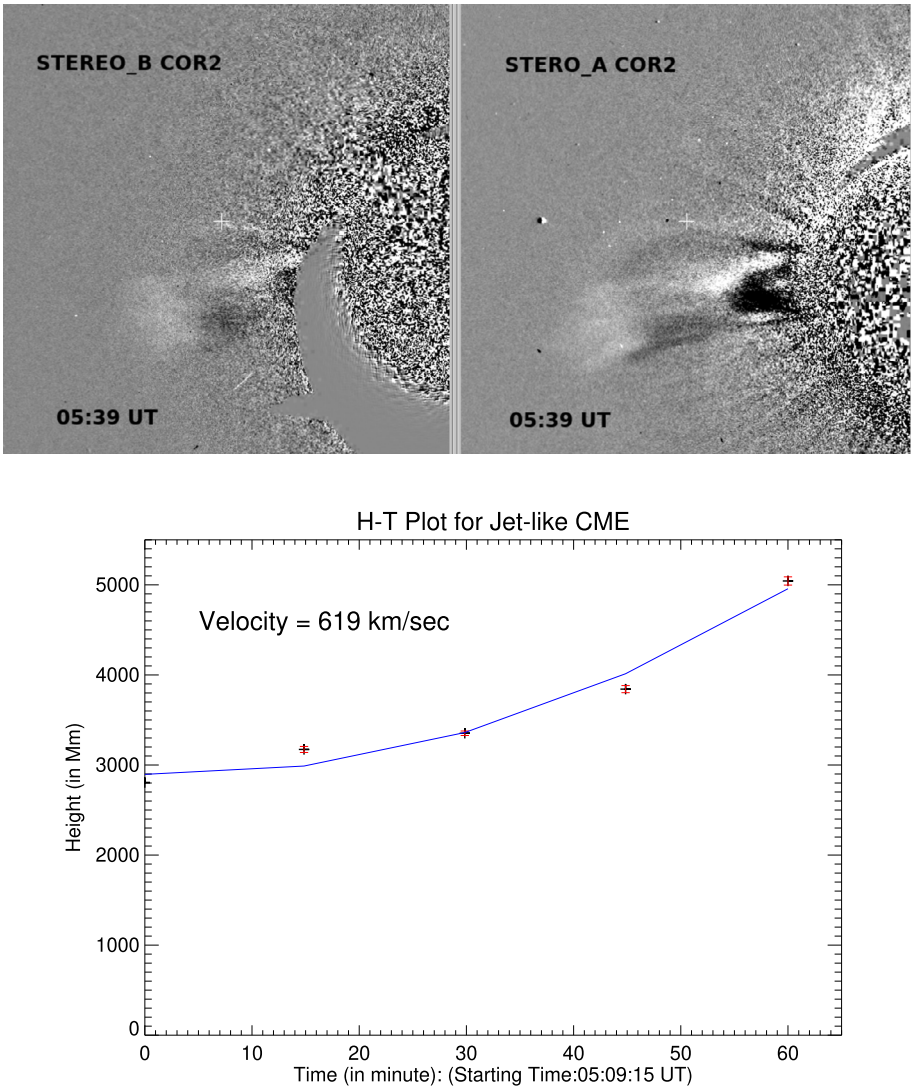

Figure 11 The *upper panel* shows the tracking of the tip of jet-like CME in STEREO_A COR2 and STEREO_B COR2 by using the triangulation technique to calculate the projected height of the CME. The *lower panel* shows the H–T plot for the jet-like CME.

M-class solar flare, where the filament eruption triggers this blowout jet. Li *et al.* (2017) observed a blowout surge in coronal loops where they found that the magnetic reconnection between the erupting filament and the coronal loop is responsible cause for the eruption of blowout surge. Shen *et al.* (2017) observed an active-region blowout jet with SDO, which was associated with a filament eruption and consisted of a hot and cool plasma structure, where the cool plasma component proceeded further than the hot plasma component. Hong *et al.* (2017) studied an active-region blowout jet associated with a C-class flare and a type-III radio burst, where it was observed that the filament eruption triggered these eruptive events. Li *et al.* (2018) recently discovered the Kelvin–Helmholtz instability in an active-

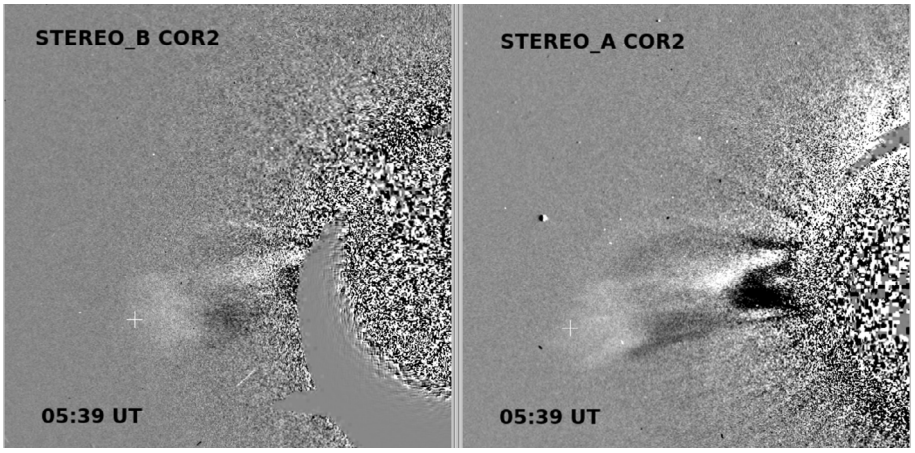

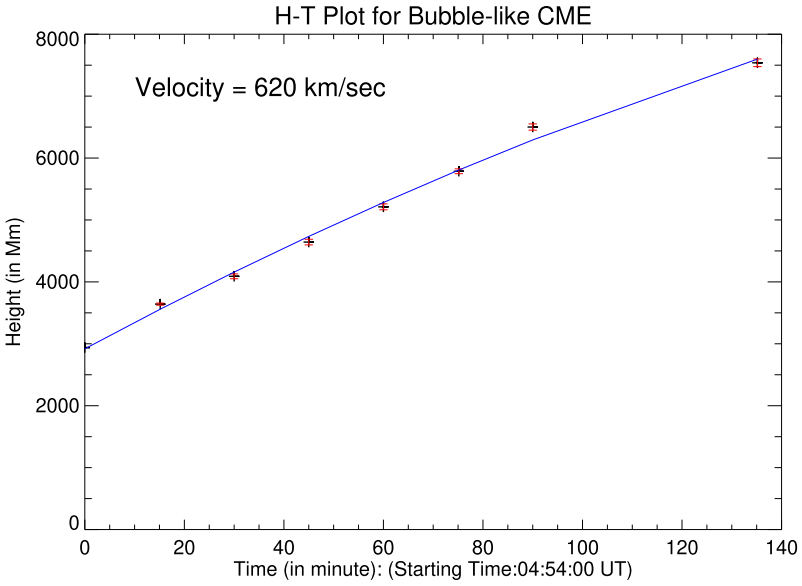

Figure 12 The *upper panel* shows the tracking of the tip of the bubble-like CME in STEREO_A COR2 and STEREO_B COR2 by using the triangulation technique to calculate the projected height of the CME. The *lower panel* shows the H–T plot for the bubble-like CME.

region penumbral structural blowout jet in the high-resolution *Interface Region Imaging Spectrograph* (IRIS) observations.

In the present work, we describe the physical properties, triggering mechanism and kinematics of a quiet-Sun blowout jet which is observed by SDO/AIA in different wavelengths on 2014 May, 16. This blowout jet is initiated by the multi-section eruptions of the circular filament which is at the base of the blowout jet. Based on our observational results, we have also found the generation of the twin CME as jet-like and bubble-like CMEs which are associated with blowout jet eruption.

Here are some concluding points of this observed event in the observed baseline studied.

i) In the time–intensity profile of the blowout jet it is observed that the cool plasma has the temperature range $\approx 10^4$–10^5 K, which is evolved earlier in the formation of the magnetised plasma spire of the blowout jet. This is due to the multiple filament ejection which further drags the blowout jet. This is a unique scenario which sheds light on the issue that the formation mechanism of this blowout jet is entirely different from the typical coronal reconnection driven blowout jets. A multi-temperature plasma and time-lagging behaviour is observed during the evolution period of the blowout jet, which is analogous with the flare eruption. We relate this flare with the network flare (Krucker *et al.*, 1997; Krucker and Benz, 2000). This flare energy accelerates the blowout jet plasma. The energisation of this network flare is due to the activation of filament segments and its reconnection with the existing overlying fields.
ii) The time evolution of the magnetic flux at the northern end of the filament is analysed and shows a magnetic cancellation signature. The magnetic cancellation destabilises the filament and further makes it erupt in different stages.
iii) The complete evolution of the blowout jet and the filament is observed in AIA 304 Å (at transition region temperature), AIA 171 Å (at inner-coronal temperature) and in Hα (at chromospheric temperature). This eruption goes through different stages as the circular filament ejects in two stages. Firstly the northern section of the filament lifts up, ejects and drives the northern part of blowout jet. In second stage the southern section of the filament also erupts and forms the rotating plasma spire of the blowout jet, *i.e.* southward part of the blowout jet.
iv) The plasma blobs are formed at the edge of the northern plasma spire of the blowout jet which are moving along the jet's spire. These plasma blobs are most likely subject to the K–H instability, which arises due to the interaction between the sheared motion of the northern part of the blowout jet and the local stationary plasma in the surrounding.
v) The velocity field is analysed at the footpoint of the northern part of the blowout jet using the Fourier Local Correlation Technique (FLCT). The velocity field shows clockwise plasma flows centred at the blowout jet triggering site, which enables the magnetic twists of similar sign in the whole northern spire of the blowout jet. This enables the sheared plasma motion in the jet's spire and most likely the evolution of K–H unstable plasma blobs.
vi) We have performed height–time analysis of the northern side of the blowout jet. The calculated velocity and acceleration are found to be 325 km s^{-1} and -0.30 km s^{-2}, respectively.
vii) Twin CMEs are observed associated with the blowout jet. The eruption of the northern part of the blowout jet drives the jet-like CME. The outward moving hot plasma on the disk is observed as the northern part of the blowout jet and in the outer coronal region it is observed as a jet-like CME. The jet-like CME is the extension of the collimated plasma beam which is generated by the external magnetic reconnection (Shen *et al.*, 2012). The eruption of the southern section of the filament enables the rotating spire of the blowout jet, which further drives the bubble-like CME. These twin CMEs are observed simultaneously.
viii) The calculated velocity and acceleration for jet-like and bubble-like CMEs are found to be 619 km s^{-1} and 0.35 km s^{-2}, 620 km s^{-1} and -0.031 km s^{-2}, respectively

In the observations of Shen *et al.* (2012) the double CMEs are less distinguishable but in our case, we can easily distinguish jet-like and bubble-like CMEs as these CMEs occur side by side. To the best of our knowledge, our observed event is the third event of the twin

CME with blowout jet eruption after the observations of the Shen *et al.* (2012) and Miao *et al.* (2018).

Acknowledgements AKS acknowledges the joint research grant under the frame-work of UKIERI (UK-India Educative and Research Initiatives). R.S. thanks the Department of Physics, Indian Institute of Technology (BHU) for providing her Senior Research Fellowship (SRF) and computational facilities. We acknowledge the SDO/AIA, SDO/HMI, SoHO/LASCO, STEREO/SECCHI, GONG Hα observations for this work. The authors acknowledge Alphonso Sterling, Navdeep Panesar, and T.V. Zaqarashvili for their fruitful discussion at initial stage and suggestions. We thank the anonymous referee for his/her valuable comments and suggestions. We thank Sudheer K. Mishra for his help in using the tie-pointing method for the kinematics of the blowout jet and twin CME.

Declaration of Potential Conflicts of Interest There was no potential conflicts of interest reported by the authors.

Publisher's Note Springer Nature remains neutral with regard to jurisdictional claims in published maps and institutional affiliations.

References

Adams, M., Sterling, A.C., Moore, R.L., Gary, G.A.: 2014, A small-scale eruption leading to a blowout macrospicule jet in an on-disk coronal hole. *Astrophys. J.* **783**, 11. DOI.

Alzate, N., Morgan, H.: 2016, Jets, coronal "puffs," and a slow coronal mass ejection caused by an opposite-polarity region within an active region footpoint. *Astrophys. J.* **823**, 129. DOI.

Brueckner, G.E., Howard, R.A., Koomen, M.J., Korendyke, C.M., Michels, D.J., Moses, J.D., Socker, D.G., Dere, K.P., Lamy, P.L., Llebaria, A., Bout, M.V., Schwenn, R., Simnett, G.M., Bedford, D.K., Eyles, C.J.: 1995, The Large Angle Spectroscopic Coronagraph (LASCO). *Solar Phys.* **162**, 357. DOI.

Chen, J., Su, J., Yin, Z., Priya, T.G., Zhang, H., Liu, J., Xu, H., Yu, S.: 2015, Recurrent solar jets induced by a satellite spot and moving magnetic features. *Astrophys. J.* **815**, 71. DOI.

Chen, P.F.: 2011, Coronal mass ejections: Models and their observational basis. *Living Rev. Solar Phys.* **8**, 1. DOI.

Domingo, V., Fleck, B., Poland, A.I.: 1995, The SOHO mission: An overview. *Solar Phys.* **162**, 1. DOI.

Fisher, G.H., Welsch, B.T.: 2008, Efficient method for performing local correlation tracking. In: *Subsurface and Atmospheric Influences on Solar Activity* **383**, 373.

Freeland, S.L., Handy, B.N.: 1998, Data analysis with the SolarSoft sYStem. *Solar Phys.* **182**, 497. DOI.

Harvey, J.W., Bolding, J., Clark, R., Hauth, D., Hill, F., Kroll, R., Luis, G., Mills, N., Purdy, T., Henney, C., Holland, D., Winter, J.: 2011, Full-disk solar H-alpha images from GONG. *Bull. Am. Astron. Soc.* **43**, 17.45.

Hong, J., Jiang, Y., Zheng, R., Yang, J., Bi, Y., Yang, B.: 2011, A micro coronal mass ejection associated blowout extreme-ultraviolet jet. *Astrophys. J.* **738**, L20. DOI.

Hong, J., Jiang, Y., Yang, J., Li, H., Xu, Z.: 2017, Minifilament eruption as the source of a blowout jet, C-class flare, and type-III radio burst. *Astrophys. J.* **835**, 35. DOI.

Howard, R.A., Moses, J.D., Vourlidas, A., Newmark, J.S., Socker, D.G., Plunkett, S.P., Korendyke, C.M., Cook, J.W., Hurley, A., Davila, J.M., Thompson, W.T., St Cyr, O.C., Mentzell, E., Mehalick, K., Lemen, J.R., Wuelser, J.P., Duncan, D.W., Tarbell, T.D., Wolfson, C.J., Moore, A., Harrison, R.A., Waltham, N.R., Lang, J., Davis, C.J., Eyles, C.J., Mapson-Menard, H., Simnett, G.M., Halain, J.P., Defise, J.M., Mazy, E., Rochus, P., Mercier, R., Ravet, M.F., Delmotte, F., Auchere, F., Delaboudiniere, J.P., Bothmer, V., Deutsch, W., Wang, D., Rich, N., Cooper, S., Stephens, V., Maahs, G., Baugh, R., McMullin, D., Carter, T.: 2008, Sun Earth Connection Coronal and Heliospheric Investigation (SECCHI). *Space Sci. Rev.* **136**, 67. DOI.

Hudson, H.S.: 2000, Implosions in coronal transients. *Astrophys. J.* **531**, L75. DOI.

Inhester, B.: 2006, Stereoscopy basics for the STEREO mission. arXiv.

Jiang, Y.C., Chen, H.D., Li, K.J., Shen, Y.D., Yang, L.H.: 2007, The Hα surges and EUV jets from magnetic flux emergences and cancellations. *Astron. Astrophys.* **469**, 331. DOI.

Jiang, Y., Shen, Y., Yi, B., Yang, J., Wang, J.: 2008, Magnetic interaction: A transequatorial jet and interconnecting loops. *Astrophys. J.* **677**, 699. DOI.

Kayshap, P., Srivastava, A.K., Murawski, K.: 2013, The kinematics and plasma properties of a solar surge triggered by chromospheric activity in AR11271. *Astrophys. J.* **763**, 24. DOI.

Kayshap, P., Srivastava, A.K., Murawski, K., Tripathi, D.: 2013, Origin of macrospicule and jet in polar corona by a small-scale kinked flux tube. *Astrophys. J.* **770**, L3. DOI.

Krucker, S., Benz, A.O.: 2000, Are heating events in the quiet solar corona small flares? Multiwavelength observations of individual events. *Solar Phys.* **191**, 341. DOI.

Krucker, S., Benz, A.O., Bastian, T.S., Acton, L.W.: 1997, X-Ray network flares of the quiet sun. *Astrophys. J.* **488**, 499. DOI.

Lemen, J.R., Title, A.M., Akin, D.J., Boerner, P.F., Chou, C., Drake, J.F., Duncan, D.W., Edwards, C.G., Friedlaender, F.M., Heyman, G.F., Hurlburt, N.E., Katz, N.L., Kushner, G.D., Levay, M., Lindgren, R.W., Mathur, D.P., McFeaters, E.L., Mitchell, S., Rehse, R.A., Schrijver, C.J., Springer, L.A., Stern, R.A., Tarbell, T.D., Wuelser, J.-P., Wolfson, C.J., Yanari, C., Bookbinder, J.A., Cheimets, P.N., Caldwell, D., Deluca, E.E., Gates, R., Golub, L., Park, S., Podgorski, W.A., Bush, R.I., Scherrer, P.H., Gummin, M.A., Smith, P., Auker, G., Jerram, P., Pool, P., Soufli, R., Windt, D.L., Beardsley, S., Clapp, M., Lang, J., Waltham, N.: 2012, The Atmospheric Imaging Assembly (AIA) on the Solar Dynamics Observatory (SDO). *Solar Phys.* **275**, 17. DOI.

Li, H., Jiang, Y., Yang, J., Qu, Z., Yang, B., Xu, Z., Bi, Y., Hong, J., Chen, H.: 2017, Blowout surge due to interaction between a solar filament and coronal loops. *Astrophys. J.* **842**, L20. DOI.

Li, X., Yang, S., Chen, H., Li, T., Zhang, J.: 2015, Trigger of a blowout jet in a solar coronal mass ejection associated with a flare. *Astrophys. J.* **814**, L13. DOI.

Li, X., Zhang, J., Yang, S., Hou, Y., Erdélyi, R.: 2018, Observing Kelvin–Helmholtz instability in solar blowout jet. *Sci. Rep.* **8**, 8136. DOI.

Liu, J., Wang, Y., Shen, C., Liu, K., Pan, Z., Wang, S.: 2015, A solar coronal jet event triggers a coronal mass ejection. *Astrophys. J.* **813**, 115. DOI.

Liu, R., Wang, H., Alexander, D.: 2009, Implosion in a coronal eruption. *Astrophys. J.* **696**, 121. DOI.

Liu, Y.: 2008, A study of surges, II: On the relationship between chromospheric surges and coronal mass ejections. *Solar Phys.* **249**, 75. DOI.

Miao, Y., Liu, Y., Li, H.B., Shen, Y., Yang, S., Elmhamdi, A., Kordi, A.S., Abidin, Z.Z.: 2018, A blowout jet associated with one obvious extreme-ultraviolet wave and one complicated coronal mass ejection event. *Astrophys. J.* **869**, 39. DOI.

Moore, R.L., Cirtain, J.W., Sterling, A.C., Falconer, D.A.: 2010, Dichotomy of solar coronal jets: Standard jets and blowout jets. *Astrophys. J.* **720**, 757. DOI.

Moore, R.L., Sterling, A.C., Falconer, D.A., Robe, D.: 2013, The cool component and the dichotomy, lateral expansion, and axial rotation of solar X-ray jets. *Astrophys. J.* **769**, 134. DOI.

Morgan, H., Druckmüller, M.: 2014, Multi-scale Gaussian normalization for solar image processing. *Solar Phys.* **289**, 2945. DOI.

Murawski, K., Srivastava, A.K., Zaqarashvili, T.V.: 2011, Numerical simulations of solar macrospicules. *Astron. Astrophys.* **535**, A58. DOI.

Ni, L., Zhang, Q.-M., Murphy, N.A., Lin, J.: 2017, Blob formation and ejection in coronal jets due to the plasmoid and Kelvin–Helmholtz instabilities. *Astrophys. J.* **841**, 27. DOI.

Nishizuka, N., Shimizu, M., Nakamura, T., Otsuji, K., Okamoto, T.J., Katsukawa, Y., Shibata, K.: 2008, Giant chromospheric anemone jet observed with hinode and comparison with magnetohydrodynamic simulations: Evidence of propagating Alfvén waves and magnetic reconnection. *Astrophys. J.* **683**, L83. DOI.

Nisticò, G., Bothmer, V., Patsourakos, S., Zimbardo, G.: 2009, Characteristics of EUV coronal jets observed with STEREO/SECCHI. *Solar Phys.* **259**, 87. DOI.

Panesar, N.K., Sterling, A.C., Moore, R.L., Chakrapani, P.: 2016, Magnetic flux cancelation as the trigger of solar quiet-region coronal jets. *Astrophys. J.* **832**, L7. DOI.

Pariat, E., Antiochos, S.K., DeVore, C.R.: 2009, A model for solar polar jets. *Astrophys. J.* **691**, 61. DOI.

Pesnell, W.D., Thompson, B.J., Chamberlin, P.C.: 2012, The Solar Dynamics Observatory (SDO). *Solar Phys.* **275**, 3. DOI.

Pucci, S., Poletto, G., Sterling, A.C., Romoli, M.: 2013, Physical parameters of standard and blowout jets. *Astrophys. J.* **776**, 16. DOI.

Raouafi, N.E., Patsourakos, S., Pariat, E., Young, P.R., Sterling, A.C., Savcheva, A., Shimojo, M., Moreno-Insertis, F., DeVore, C.R., Archontis, V., Török, T., Mason, H., Curdt, W., Meyer, K., Dalmasse, K., Matsui, Y.: 2016, Solar coronal jets: Observations, theory, and modeling. *Space Sci. Rev.* **201**, 1. DOI.

Scherrer, P.H., Schou, J., Bush, R.I., Kosovichev, A.G., Bogart, R.S., Hoeksema, J.T., Liu, Y., Duvall, T.L., Zhao, J., Title, A.M., Schrijver, C.J., Tarbell, T.D., Tomczyk, S.: 2012, The Helioseismic and Magnetic Imager (HMI) investigation for the Solar Dynamics Observatory (SDO). *Solar Phys.* **275**, 207. DOI.

Shen, Y., Liu, Y., Su, J.: 2012, Sympathetic partial and full filament eruptions observed in one solar breakout event. *Astrophys. J.* **750**, 12. DOI.

Shen, Y., Liu, Y., Su, J., Ibrahim, A.: 2011, Kinematics and fine structure of an unwinding polar jet observed by the Solar Dynamic Observatory/Atmospheric Imaging Assembly. *Astrophys. J.* **735**, L43. DOI.

Shen, Y., Liu, Y., Su, J., Deng, Y.: 2012, On a coronal blowout jet: The first observation of a simultaneously produced bubble-like CME and a jet-like CME in a solar event. *Astrophys. J.* **745**, 164. DOI.
Shen, Y., Liu, Y.D., Su, J., Qu, Z., Tian, Z.: 2017, On a solar blowout jet: Driving mechanism and the formationof cool and hot components. *Astrophys. J.* **851**, 67. DOI.
Shen, Y., Tang, Z., Li, H., Liu, Y.: 2018a, Coronal EUV, QFP, and kink waves simultaneously launched during the course of jet–loop interaction. *Mon. Not. Roy. Astron. Soc.* **480**, L63. DOI.
Shen, Y., Tang, Z., Miao, Y., Su, J., Liu, Y.: 2018b, EUV waves driven by the sudden expansion of transequatorial loops caused by coronal jets. *Astrophys. J.* **860**, L8. DOI.
Shen, Y., Liu, Y., Liu, Y.D., Su, J., Tang, Z., Miao, Y.: 2018c, Homologous large-amplitude nonlinear fast-mode magnetosonic waves driven by recurrent coronal jets. *Astrophys. J.* **861**, 105. DOI.
Shibata, K., Nishikawa, T., Kitai, R., Suematsu, Y.: 1982, Numerical hydrodynamics of the jet phenomena in the solar atmosphere. *Solar Phys.* **77**, 121. DOI.
Shibata, K., Ishido, Y., Acton, L.W., Strong, K.T., Hirayama, T., Uchida, Y., McAllister, A.H., Matsumoto, R., Tsuneta, S., Shimizu, T., Hara, H., Sakurai, T., Ichimoto, K., Nishino, Y., Ogawara, Y.: 1992, Observations of X-ray jets with the YOHKOH Soft X-ray telescope. *Publ. Astron. Soc. Japan* **44**, L173.
Shibata, K., Nitta, N., Strong, K.T., Matsumoto, R., Yokoyama, T., Hirayama, T., Hudson, H., Ogawara, Y.: 1994, A gigantic coronal jet ejected from a compact active region in a coronal hole. *Astrophys. J.* **431**, L51. DOI.
Shibata, K., Nakamura, T., Matsumoto, T., Otsuji, K., Okamoto, T.J., Nishizuka, N., Kawate, T., Watanabe, H., Nagata, S., UeNo, S., Kitai, R., Nozawa, S., Tsuneta, S., Suematsu, Y., Ichimoto, K., Shimizu, T., Katsukawa, Y., Tarbell, T.D., Berger, T.E., Lites, B.W., Shine, R.A., Title, A.M.: 2007, Chromospheric anemone jets as evidence of ubiquitous reconnection. *Science* **318**, 1591. DOI.
Shimojo, M., Shibata, K., Harvey, K.L.: 1998, Magnetic field properties of solar X-ray jets. *Solar Phys.* **178**, 379. DOI.
Shimojo, M., Hashimoto, S., Shibata, K., Hirayama, T., Hudson, H.S., Acton, L.W.: 1996, Statistical study of solar X-ray jets observed with the Yohkoh Soft X-Ray telescope. *Publ. Astron. Soc. Japan* **48**, 123. DOI.
Solanki, R., Srivastava, A.K., Dwivedi, B.N.: 2018, Study of two-stage coronal jet associated with a C1.4 class solar flare. *Astrophys. Space Sci.* **363**, 233. DOI.
Srivastava, A.K., Murawski, K.: 2011, Observations of a pulse-driven cool polar jet by SDO/AIA. *Astron. Astrophys.* **534**, A62. DOI.
Sterling, A.C., Moore, R.L., Falconer, D.A., Adams, M.: 2015, Small-scale filament eruptions as the driver of X-ray jets in solar coronal holes. *Nature* **523**, 437. DOI.
Tian, Z., Liu, Y., Shen, Y., Elmhamdi, A., Su, J., Liu, Y.D., Kordi, A.S.: 2017, Successive two-sided loop jets caused by magnetic reconnection between two adjacent filamentary threads. *Astrophys. J.* **845**, 94. DOI.
Uddin, W., Schmieder, B., Chandra, R., Srivastava, A.K., Kumar, P., Bisht, S.: 2012, Observations of multiple surges associated with magnetic activities in AR 10484 on 2003 October 25. *Astrophys. J.* **752**, 70. DOI.
Wang, Y.-M., Sheeley, N.R. Jr., Socker, D.G., Howard, R.A., Brueckner, G.E., Michels, D.J., Moses, D., St. Cyr, O.C., Llebaria, A., Delaboudinière, J.-P.: 1998, Observations of correlated white-light and extreme-ultraviolet jets from polar coronal holes. *Astrophys. J.* **508**, 899. DOI.
Wuelser, J.-P., Lemen, J.R., Tarbell, T.D., Wolfson, C.J., Cannon, J.C., Carpenter, B.A., Duncan, D.W., Gradwohl, G.S., Meyer, S.B., Moore, A.S., Navarro, R.L., Pearson, J.D., Rossi, G.R., Springer, L.A., Howard, R.A., Moses, J.D., Newmark, J.S., Delaboudiniere, J.-P., Artzner, G.E., Auchere, F., Bougnet, M., Bouyries, P., Bridou, F., Clotaire, J.-Y., Colas, G., Delmotte, F., Jerome, A., Lamare, M., Mercier, R., Mullot, M., Ravet, M.-F., Song, X., Bothmer, V., Deutsch, W.: 2004 EUVI: The STEREO-SECCHI extreme ultraviolet imager. In: *Telescopes and Instrumentation for Solar Astrophysics* **5171**, 111. DOI.
Yokoyama, T., Shibata, K.: 1995, Magnetic reconnection as the origin of X-ray jets and Hα surges on the Sun. *Nature* **375**, 42. DOI.
Zhelyazkov, I., Chandra, R.: 2018, High mode magnetohydrodynamic waves propagation in a twisted rotating jet emerging from a filament eruption. *Mon. Not. Roy. Astron. Soc.* **478**, 5505. DOI.
Zhelyazkov, I., Zaqarashvili, T.V., Ofman, L., Chandra, R.: 2018, Kelvin–Helmholtz instability in a twisting solar polar coronal hole jet observed by SDO/AIA. *Adv. Space Res.* **61**, 628. DOI.
Zhu, X., Wang, H., Cheng, X., Huang, C.: 2017, A solar blowout jet caused by the eruption of a magnetic flux rope. *Astrophys. J.* **844**, L20. DOI.